

Spin-entropy driven melting of the charge order in $\text{La}_{1.5}\text{Sr}_{0.5}\text{CoO}_4$.

I. A. Zaliznyak¹, J. M. Tranquada¹, R. Erwin², Y. Moritomo³

¹*Department of Physics, Brookhaven National Laboratory, Upton, New York 11973-5000*

²*National Institute of Standards and Technology, Gaithersburg, Maryland 20899*

³*Center for Integrated Research in Science and Engineering (CIRSE), Nagoya University, Nagoya 464-8601, Japan*

(October 27, 2018)

We studied the melting of the charge order in the half-doped tetragonal perovskite $\text{La}_{1.5}\text{Sr}_{0.5}\text{CoO}_4$ by elastic neutron scattering. We found that diffuse peaks, corresponding to the breathing-type modulation of oxygen positions in the CoO_6 octahedra, disappear above $T_c = 825(27)$ K. This melting of the diffuse superstructure is reversible (no change in the correlation lengths upon annealing is observed) and accompanied by a large nonlinear thermal expansion along the tetragonal c -axis, with a cusp at T_c . We conclude that quenched disorder of the doped Sr ions is at the origin of this *anisotropic charge glass* state. We also suggest that its melting is driven by the transition from the intermediate- to the high-spin state of Co^{3+} ion, which is favored by the spin entropy at high T .

PACS numbers: 71.28.+d 71.45.Lr 75.40.Gb,

Understanding the cooperative charge ordered phases in doped transition-metal oxides is a key problem in the physics of colossal-magnetoresistance (CMR) materials and high-temperature superconductors.^{1,2} Electron correlations in these systems are driven by contributions from several equally important interactions, such as Hund's coupling, splitting of the on-site electronic levels by the crystal field, Jahn-Teller (JT) distortion, Coulomb repulsion between the conduction electrons, superexchange, double exchange, *etc.* Competing ground states lead to a rich variety of phases, depending on the electronic configuration of the 3d metal ion, its crystal environment, the doping level, and so on. To understand, and ultimately predict, the nature and the physical properties of a given transition-metal oxide at a particular doping, it is extremely important to study the origin of, and the relation between, charge order (CO), spin order (SO) and orbital order (OO) in different compounds.

The case of half-doping, which is relevant for the CMR materials, is of special interest for several reasons. First, the spatial structure of the CO instability is particularly simple – it is a checkerboard-type arrangement of the doped charges in the tetragonal plane. Second, it is argued to be of most technological relevance in perovskite manganites.³ Finally, an orbital order, concomitant with CO, was recently directly observed in several half-doped manganites by X-ray resonant scattering.^{4,5} Consequently, a number of theoretical papers appeared, aimed at explaining the origin of the observed CO/OO at half-doping, its relation with spin order and implications for the transport properties.^{6–8} To verify these theories, and eventually achieve clear understanding of this important problem, more experimental input is vital.

In a recent neutron scattering study⁹ we characterized spin and charge order in the half-doped cobaltate $\text{La}_{1.5}\text{Sr}_{0.5}\text{CoO}_4$. We found that the spins order at $T_s \approx 30$ K in a quasi-two-dimensional incommensurate glassy structure, while checkerboard short-range CO persists to at least ~ 600 K and shows no measurable anomaly

at T_s , *i.e.* the freezing of charge and spin correlations are independent instabilities, inherent to the electronic and crystal structure of $\text{La}_{1.5}\text{Sr}_{0.5}\text{CoO}_4$. Both magnetic and structural scattering were similar to those observed in the isostructural manganite $\text{La}_{0.5}\text{Sr}_{1.5}\text{MnO}_4$,¹⁰ where CO and SO transition temperatures are much closer, and corresponding instabilities are often presumed to be closely related. The main difference in our case is the much shorter coherence range: correlations within the tetragonal $\mathbf{a-b}$ planes extend only over $\xi_s \sim 80$ Å for SO, and less than $\xi_{\text{co}} \sim 30$ Å for CO, while $\xi_{\text{co}} \gtrsim 200$ Å in $\text{La}_{0.5}\text{Sr}_{1.5}\text{MnO}_4$.¹² Despite its short-range glassy nature, CO in $\text{La}_{1.5}\text{Sr}_{0.5}\text{CoO}_4$ has no less drastic consequences for transport properties than that in manganite,¹⁰ resulting in an insulating state, and an activation behavior of the electrical conductivity with $E_a \sim 6000$ K.¹³ In fact, such an apparently large activation energy (*i.e.* a weak temperature dependence of the conductivity), is observed in the pseudo-cubic perovskite cobaltites RCoO_3 , $\text{R}=\text{La,Pr,Nd,Sm,Eu,Gd}$ at temperatures 400 – 600 K,¹⁴ where a semiconductor-to-metal cross-over occurs upon heating. Comparative studies of the isostructural Co and Mn compounds give a unique opportunity to understand the relative importance of the anisotropic crystal field energy, which in the cobaltites can be larger than the on-site Hund's coupling, and the inter-site spin interaction, which is often quenched for the Co^{3+} ions.^{9,15}

Here we focus our attention on the nature of the CO glassy state and the charge melting process in $\text{La}_{1.5}\text{Sr}_{0.5}\text{CoO}_4$. We study the temperature evolution of the CO correlation lengths and the charge order parameter up to and above T_c , and investigate the effect of annealing and slow cooling of the sample through the CO transition. Such procedure could distinguish between the cooling-rate-dependent disorder of the mobile ions (non-stoichiometric oxygen) or charge carriers, which can reorder into an equilibrium arrangement,¹¹ and that related to the quenched disorder of the immobile Sr^{2+} ions.

We studied the same high quality single crystal sam-

ple of $\text{La}_{1.5}\text{Sr}_{0.5}\text{CoO}_4$ as in Ref. 9. At all temperatures the crystal remained in the tetragonal “HTT” phase (space group $I4/mmm$), with low T lattice parameters $a = 3.83 \text{ \AA}$ and $c = 12.5 \text{ \AA}$, Fig. 1(a). In Ref. 9 we used the “orthorhombic” indexing, based on the space group $F4/mmm$ with a unit cell that is two times larger. This accounts for breaking of the translational symmetry in the \mathbf{a} - \mathbf{b} plane by the checkerboard CO superstructure, and is convenient for describing the spin order. Here, however, we will use the “HTT” $I4/mmm$ notation,¹⁰ which is relevant for the charge-disordered phase, and is more appropriate for characterizing the CO instability.

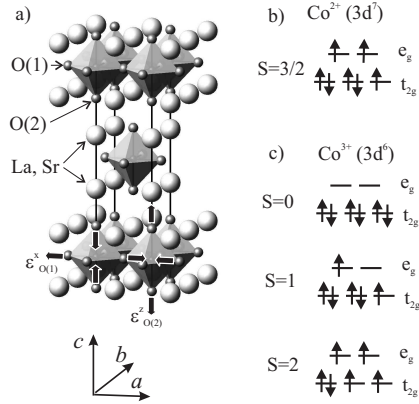


FIG. 1. (a) Crystal structure of $\text{La}_{1.5}\text{Sr}_{0.5}\text{CoO}_4$, arrows show the directions of oxygen displacements $\epsilon_{O(1),O(2)}$ accompanying the CO modulation. (b),(c) Filling of the electronic levels in (b) Co^{2+} with $S=3/2$, and (c) in Co^{3+} in the LS ($S=0$), IS ($S=1$) and HS ($S=2$) states.

Experiments were performed on BT2, BT4 and BT9 thermal beam 3-axis neutron spectrometers at NIST Center for Neutron Research. PG(002) reflections were used at the monochromator and analyzer, supplemented by two PG filters to suppress the contamination from the higher order reflections. The energy of the scattered neutrons was fixed at $E_f = 14.7 \text{ meV}$, beam collimations were $80' - 42' - 62' - 100'$ on BT2 and BT4, and $40' - 56' - 51' - 100'$ on BT9. The cylindrical sample was mounted either in a displax refrigerator or in a 850 K vacuum furnace (BT9) with the axis vertical, allowing wavevector transfers in the (hhl) reciprocal lattice plane. Some scans on BT9 were also done at ambient in the $(hk0)$ plane. Sample mosaic is $\lesssim 0.25^\circ$ in the (hhl) plane, and $\lesssim 0.4^\circ$ in the $(hk0)$ plane. Normalization of the scattering intensity was performed using the incoherent scattering from a vanadium standard.

An extensive survey of elastic scattering from the super-structure induced by the CO is presented in Fig. 2. It consists of broad commensurate peaks centered at $Q = (h + 0.5, k + 0.5, l)$ reciprocal lattice units (rlu) with h, k, l integer, which corresponds to a checkerboard arrangement of the $\text{Co}^{2+}/\text{Co}^{3+}$ valence in the \mathbf{a} - \mathbf{b} plane. An increase in the intensity at large Q , characteristic of the scattering from a structural modulation, is apparent.

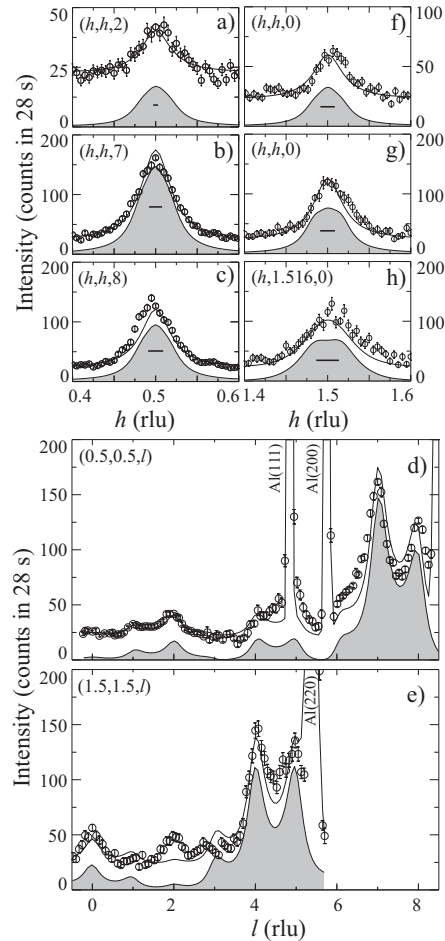


FIG. 2. Elastic scattering from the diffuse structural modulation accompanying charge order in $\text{La}_{1.5}\text{Sr}_{0.5}\text{CoO}_4$. (a)-(f) scans collected on BT2 at $T = 6 \text{ K}$ in the (hhl) reciprocal plane. (g),(h) scans collected on BT9 at ambient $T \approx 295 \text{ K}$ in the $(hk0)$ reciprocal plane. Horizontal bars show the full width at half maximum (FWHM) of the spectrometer elastic resolution along the scan direction. Solid curves through the data are the resolution corrected fits to the single peak cross-section (1). Shaded peaks show the net intensity which would result from four incommensurate peaks at $Q_c = \{(0.5 \pm \epsilon, 0.5 \pm \epsilon, l), (0.5 \pm \epsilon, 0.5 \mp \epsilon, l)\}$ with $\epsilon = 0.016$.

In all scans the widths of the peaks are substantially larger than the instrument elastic resolution, which reveals the short-range nature of the CO. The peaks are broader in the \mathbf{c} -axis direction, so that the super-structure is an anisotropic glass with the correlation extending by about 4 lattice repeats in the \mathbf{a} - \mathbf{b} plane, and only $2/3$ of a lattice repeat along the \mathbf{c} axis, *i.e.* only between the two nearest CoO_4 planes. The intensity modulation with l shown in the Fig. 2 (d), (e), exhibits a rather peculiar long-periodic pattern, which translates into a modulation of a small object in real space. In Ref. 9 we showed that scattering from a breathing-type distortion of the oxygen octahedra surrounding the Co ions provided a good account of a smaller set of data. This involves displacements of the in-plane oxygens $\epsilon_{O(1)}^{x,y}$,

and apical oxygens $\varepsilon_{O(2)}^z$, along the corresponding Co-O bonds, as shown in Fig. 1 (a). The neutron scattering elastic cross-section arising from such a modulation, short-range-periodic in the crystal lattice, has the form of the factorized “lattice Lorentzians”,¹⁶

$$\frac{d\sigma}{d\Omega}(\mathbf{q}) = NI_{DW} |F(\mathbf{q})|^2 \frac{1}{n_{\pm}} \sum_{+,-} \mathcal{L}_a^{\pm}(\mathbf{q}) \mathcal{L}_b^{\pm}(\mathbf{q}) \mathcal{L}_c^{\pm}(\mathbf{q}), \quad (1)$$

$$\mathcal{L}_a^{\pm}(\mathbf{q}) = \frac{\sinh \xi_a^{-1}}{\cosh \xi_a^{-1} - \cos(\mathbf{q} \pm \mathbf{Q}) \cdot \mathbf{a}}, \quad \text{etc.} \quad (2)$$

Here $F(\mathbf{q}) = \sum_{\mu} (\mathbf{q} \cdot \boldsymbol{\varepsilon}_{\mu}) b_{\mu} e^{-i(\mathbf{q} \cdot \mathbf{r}_{\mu})}$, N is the number of unit cells in the crystal, I_{DW} is an effective Debye-Waller intensity prefactor, $\boldsymbol{\varepsilon}_{\mu}$ is the displacement of the atom μ inside a unit cell from its nominal position \mathbf{r}_{μ} , b_{μ} is its scattering length, \mathbf{Q} is the modulation wavevector, $\xi_a = \xi_b = \xi_h$ and $\xi_c = \xi_l$ are the in-plane and inter-plane correlation lengths measured in lattice units (lu), and n_{\pm} is the number of terms in the last summation.

We performed a global fit of all measured intensities at each T with Eq. (1), corrected for the instrument resolution, and implying an equal-weight superposition of the commensurate modulations with $\mathbf{Q} = (0.5, 0.5, l)$ for $l = 0, 1$. This corresponds to an equal probability for the in-phase and anti-phase stacking of the checkerboard CO structure for neighboring planes along c . At low temperatures the Debye-Waller factor was fixed at $I_{DW} = 1$, and the displacements of the O nuclei from the nominal positions $r_{O(1)} = (0.5, 0, 0)$, $(0, 0.5, 0)$ lu and $r_{O(2)} = (0, 0, 0.173)$ lu, the correlation lengths ξ_h and ξ_l , the background from the \mathbf{q} -independent incoherent elastic scattering and the Bragg scattering by the polycrystalline aluminum in the sample environment were refined. Adding a modulation of the La/Sr position, $r_{La,Sr} = (0.5, 0.5, 0.141)$ lu, as well as varying $z_{O(2)}$ and $z_{La,Sr}$, did not improve the quality of the fit. The solid lines through the data in the panels of Fig. 2 result from Eq. (1) with parameters obtained in the global fit and summarized in the Table 1. Clearly, the scattering from the oxygen displacements gives a very good description of all measured intensities.

In the Ref. 9 we also found magnetic elastic scattering which appears below $T \approx 30$ K at slightly incommensurate positions $Q_m = (\frac{0.5+\epsilon}{2}, \frac{0.5+\epsilon}{2}, l)$ with $\epsilon \approx 0.016$ and l odd-integer. If this incommensurability of the spin order is the result of a stripe order of the doped charges, related to a small deviation of the La:Sr ratio from the nominal 1.5:0.5, or some non-stoichiometric oxygen, we would also expect four incommensurate CO peaks at $Q_c = \{(0.5 \pm \epsilon, 0.5 \pm \epsilon, l), (0.5 \pm \epsilon, 0.5 \mp \epsilon, l)\}$, as observed in the doped cuprates.¹⁷ However, for the scans in the (h, h, l) plane, Fig. 2 (a)-(f), the major contribution of the out-of-plane peaks, accepted by the coarse vertical resolution of the spectrometer and centered at $h = 0.5$, would hinder the experimental observation of the incommensurate splitting.⁹ To clarify this issue we made a number of scans through the CO scat-

tering around $(1.5, 1.5, 0)$ and $(2.5, 0.5, 0)$ in the $(h, k, 0)$ plane. No splitting was apparent in any of these scans either, as illustrated by two representative datasets in Fig. 2 (g),(h). The overall peak width is always dominated by the short correlation length, which smears the implied small splitting. In other words, the correlation range of the CO, $\xi_h \approx 4$ lu, is so small compared to the wavelength of the expected incommensurate modulation $\lambda_{\epsilon} = 1/\epsilon \approx 60$ lu, that the latter is undetectable. The cross-section resulting from four incommensurate peaks with $\epsilon = 0.016$ is shown by the shaded areas in the Fig. 2. It gives an almost identical fit to the measured intensities, with only a slightly larger ξ_h to “compensate” for the splitting, see Table 1.

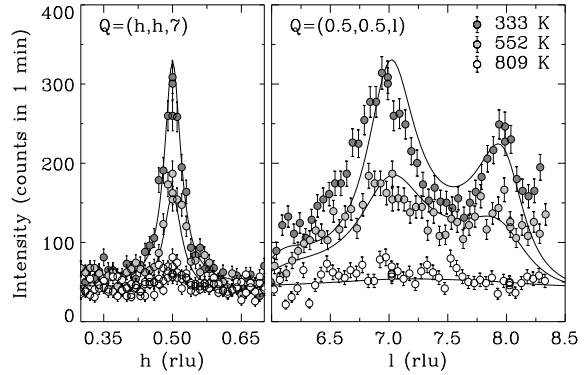


FIG. 3. Change in the diffuse super-structural scattering concomitant with melting of the CO in $\text{La}_{1.5}\text{Sr}_{0.5}\text{CoO}_4$.

Figure 3 shows the evolution of the diffuse CO scattering upon heating. Although a small peak may still be present in the h -scan at $T = 809$ K, we find that it completely disappears at 850 K. Each measurement at high T was preceded by a sample re-alignment, since the melting of the charge order in $\text{La}_{1.5}\text{Sr}_{0.5}\text{CoO}_4$ is accompanied by an anomalously large thermal expansion along the c -axis, Fig. 4(a). We find that the temperature dependence $c(T)$ saturates somewhere above 800 K, with a kink indicative of a second order phase transition. This supports our suggestion⁹ that the decrease in the c lattice spacing below T_c is proportional to the charge order parameter η_c . Fitting it with the expression $c(T) = c(850 \text{ K}) - \alpha(T_c - T)^\beta$ we get $T_c = 825(27)$ K and $\beta = 0.59(15)$, indistinguishable from the mean-field value 0.5. The in-plane lattice constant a , on the other hand, stays almost unchanged, with some tendency to decrease upon heating, and exhibits no anomaly at T_c . These findings clearly indicate that electrons involved in the CO are localized in the out-of-plane $d_{3z^2-r^2}$ orbitals.

Interestingly, to within our errors the width of the peak in h does not change upon heating, i.e. the in-plane correlation length stays constant, and CO melting mostly involves the loss of the inter-plane coherence with increasing T , Fig.4 (b). In the fits of the scans for $T > 300$ K we fixed the oxygen displacements and varied the “Debye-Waller” prefactor to account for the decrease in the CO scattering intensity, which follows the disappearance of

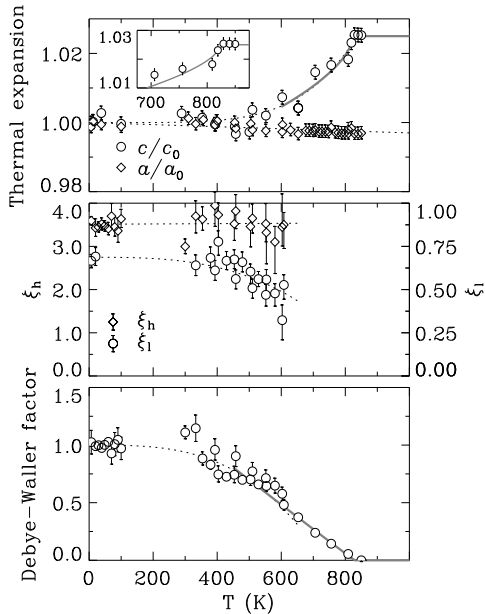


FIG. 4. Temperature dependence of the structural parameters related to the CO in $\text{La}_{1.5}\text{Sr}_{0.5}\text{CoO}_4$. (a) change of the lattice constants relative to the low- T values. (b) in-plane (left scale) and inter-plane (right scale) correlation length, for $T \geq 650$ K they were fixed at $\xi_h = 3.5$ lu, $\xi_l = 0.32$ lu. (c) intensity (“Debye-Waller”) prefactor. Broken curves are the guides for the eye, solid lines are the critical-law fits (see text).

the order parameter η_c , Fig. 4(c). The solid line in Fig. 4(c) is the best fit to the expression $I_{DW}(T) \sim (T_c - T)^\gamma$, which gives $T_c = 821(48)$ K, identical with that refined from the $c(T)$, and $\gamma = 0.92(11)$. The exponent γ agrees well with $\gamma = 2\beta$, expected from $I_{DW} \sim \eta_c^2$, and also with the mean-field value $\gamma = 1$.

We found that upon slow cooling, even after annealing the sample for a few hours at $T = 850$ K, the CO peaks reappear below T_c with the same width and intensity as before. The reversible nature of the melting transition is important for understanding the origin of the *charge glass* phase in $\text{La}_{1.5}\text{Sr}_{0.5}\text{CoO}_4$. It suggests that the quenched disorder of the dopant Sr ions, which strongly interact with the doped charges, is the most probable cause for the loss of the CO in-plane coherence, and not a non-stoichiometric oxygen or rapid quench through T_c .

A key for understanding the $\text{Co}^{3+}/\text{Co}^{2+}$ mixed valence phases and cobaltites in general is provided by the peculiar structure of the $3d$ electron levels. In a cubic crystal field $3d$ levels are split into a lower t_{2g} triplet and an e_g doublet of $d_{x^2-y^2}$ and $d_{3z^2-r^2}$ orbitals. In cobalt the Hund splitting of spin “up” and “down” $3d$ levels is anomalously small, and though Co^{2+} ($3d^7$) is in the “normal” $S=3/2$ state $t_{2g}^5 e_g^2$, Fig. 1(b), Co^{3+} ($3d^6$) may be found in either the high $t_{2g}^4 e_g^2$ (HS, $S=2$), intermediate $t_{2g}^5 e_g^1$ (IS, $S=1$), or low spin state t_{2g}^6 (LS, $S=0$), Fig. 1(c). If LS were the ground state, as in LaCoO_3 , a decrease in the free energy $F = E - T \ln(2S + 1)$ due to the higher paramagnetic entropy may drive transitions to IS and

HS states with increasing temperature.^{15,18} On the other hand, it is clear from Figure 1(c) that only the IS $S=1$ state is JT-active, *i.e.* favors tetragonal splitting of the e_g doublet, as it has one electron there. In either the HS or LS state, such splitting gains no energy because both e_g levels are equally occupied.

We conclude, that Co^{3+} ions in $\text{La}_{1.5}\text{Sr}_{0.5}\text{CoO}_4$ are in the IS state at low T , which favors the JT-distorted CO phase. At higher T , a spin-entropy driven transition to the HS state occurs (similar IS-HS transition is observed in LaCoO_3 at ≈ 600 K¹⁵) with consequent disappearance of the JT modulation and conspicuous melting of the charge order. Therefore, it appears that local effects such as the spin-state transition and JT level splitting are very important and quite efficient in driving the CO phase in $\text{La}_{1.5}\text{Sr}_{0.5}\text{CoO}_4$, and, perhaps, in other materials.

We thank NIST Center for neutron Research for hospitality, and J. P. Hill for valuable remarks. This work was carried out under Contract NO. DE-AC02-98CH10886, Division of materials Sciences, US Department of Energy.

- 1 J. Orenstein and A. J. Millis, *Science* **288**, 468 (2000).
- 2 Y. Tokura and N. Nagaosa, *Science* **288**, 462 (2000).
- 3 P. Shiffer *et al.*, *Phys. Rev. Lett.* **75**, 3336 (1995).
- 4 Y. Murakami *et al.*, *Phys. Rev. Lett.* **80**, 1932 (1998).
- 5 M. v. Zimmerman *et al.*, *Phys. Rev. Lett.* **83**, 4872 (1999); Z. Jirák *et al.*, *Phys. Rev. B* **61**, 1181 (2000).
- 6 I. V. Solovyev and K. Terakura, *Phys. Rev. Lett.* **83**, 2825 (1999); J. van den Brink *et al.*, *Phys. Rev. Lett.* **83**, 5118 (1999).
- 7 C. N. A. van Duin and J. Zaanen, *Phys. Rev. Lett.* **80**, 1513 (1998).
- 8 G. Jackeli *et al.*, *Phys. Rev. B* **62**, 372 (1999).
- 9 I. A. Zaliznyak *et al.*, *Phys. Rev. Lett.* **85**, 4353 (2000).
- 10 B. J. Sternlieb *et al.*, *Phys. Rev. Lett.* **76**, 2169 (1996).
- 11 B. O. Wells *et al.*, *Science* **277**, 1067 (1997).
- 12 Y. Wakabayashi *et al.*, *J. Phys. Soc. Jpn.* (in press).
- 13 Y. Moritomo *et al.*, *Phys. Rev. B* **55**, R14725 (1997).
- 14 S. Yamaguchi *et al.*, *Phys. Rev. B* **54**, R11022 (1996).
- 15 K. Asai *et al.*, *J. Phys. Soc. Jpn.* **67**, 290 (1998).
- 16 M. E. Fisher, *Am. J. Phys.* **32**, 343 (1964).
- 17 J. M. Tranquada *et al.*, *Phys. Rev. Lett.* **78**, 338(1997); *Phys. Rev. B* **59**, 14712 (1999).
- 18 T. Saitoh *et al.*, *Phys. Rev. B* **55**, 4257 (1997).

TABLE I. Correlation lengths and oxygen displacements (lu) obtained from the global fit of the measured CO scattering at $T < 300$ K with the Eq. (1), ϵ is an implied incommensurability of the CO in the $\mathbf{a-b}$ plane (lu).

ϵ	$\epsilon_{O(1)}^{x,y}$	$\epsilon_{O(2)}^z$	ξ_h	ξ_l
0	0.012(1)	-0.0058(4)	3.7(3)	0.67(5)
0.016	0.012(1)	-0.0057(3)	4.9(6)	0.65(4)